Fizika Nizkikh Temperatur, 2008, v. 34, No. 10, p. 1033–1039

Effect of next-to-nearest neighbor hopping on electronic properties of graphene

Y.F. Suprunenko[1,2], E.V. Gorbar[1], S.G. Sharapov[3], and V.M. Loktev[1]

[1]*Bogolyubov Institute for Theoretical Physics of the National Academy of Sciences of Ukraine*
14-b Metrolohichna Str., Kiev 03680, Ukraine
E-mail:vloktev@bitp.kiev.ua

[2]*Physics Department, Lancaster University, Lancaster, LA1 4YB, UK*

[3]*Physics Department, Western Illinois University, Macomb, Illinois 61455, USA*
E-mail:s-sharapov@wiu.edu

Received April 2, 2008

In the tight-binding approximation, we take into account the next-to-nearest neighbor hopping in graphene that leads to nonrelativistic-like corrections in its low energy spectrum. The electronic density of states in a magnetic field is found and the fan diagram is plotted, which interpolates between those for the relativistic and nonrelativistic limiting cases. It is shown that the Berry phase for the system under consideration coincides exactly with its value for the relativistic system.

PACS: **71.70–d** Level splitting and interactions;
81.05.Uw Carbon, diamond, graphite.

Keywords: graphene, electron density of states, magnetic field, Berry phase.

Introduction

Since the discovery of graphene [1] and especially the experimental observation [2,3] and theoretical prediction [4–7] of an anomalous quantization in the quantum Hall effect (QHE), studies of graphene present an extremely active and even separate branch of research in the modern condensed matter physics.

Graphene is a single-atom thick two-dimensional plane of graphite. The honeycomb lattice of graphene (see Fig. 1) can be considered as composed of two triangular sublattices A and B. In 1947, Wallace [8] in the tight-binding approximation considered graphene as a building block of graphite taking into account only the nearest neighbor π-electron hopping. According to Fig. 1, the vectors ρ_{AB} describe this hopping between two sublattices of graphene. Wallace showed that graphene's 2D nature and honeycomb atomic structure cause electrons to move as if they have no mass (they are described by the Dirac equation [9]). Indeed, at low energy the band structure of graphene is formed from the π-electron carbon orbitals and consists of a valence (full) and conduction (empty) bands both conical in shape with vertex meeting at a point called a Dirac point. There are two nonequivalent pairs of such cones. The low energy spectrum of the π-electrons is given by a relativistic-like relation $E = \pm \hbar v_F |\mathbf{k}|$ for massless particles, where the Fermi velocity v_F is approximately 300 times smaller than the speed of light c, and $\mathbf{k}$ is quasiparticle wavevector.

The experimental proof of the existence of Dirac fermions in graphene came from the observation [2,3] of the unconventional QHE. The reason for the occurrence of odd integers is connected with a quantum-mechanical effect called the Berry phase [10], which equals π for

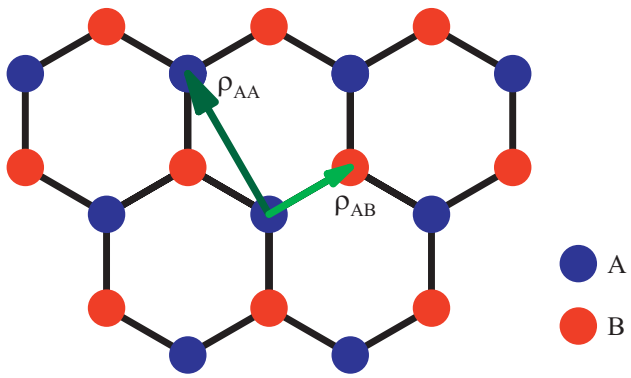

Fig. 1. Graphene's honeycomb lattice and vectors of the nearest and next-to-nearest neighbor hoppings.

graphene. This value of the Berry phase was obtained in the original paper Ref. 10 for a toy model. This model can be derived from the tight-binding consideration of graphene taking into account the nearest neighbor hopping only. For a recent discussion of the Berry phase in graphene see [11].

This hopping is the leading term contribution in graphene. There is also the next-to-nearest neighbor hopping denoted by the ρ_{AA} (or ρ_{BB}) vectors in Fig. 1. Its effect on the energy spectrum in a constant magnetic field was already considered in [7,12], where it was shown that such a hopping breaks the electron-hole symmetry of the Dirac spectrum and produces terms characteristic for a nonrelativistic problem.

In the present paper, we will consider in more detail how the next-to-nearest neighbor hopping affects the electronic properties of two-dimensional systems with honeycomb lattice. In Sec. 2, we repeat the derivation of the energy spectrum in a constant magnetic field. In Sec. 3, we calculate the density of states (DOS). Fan diagrams are plotted in Sec. 4. Conclusions are given in Sec. 5.

2. The energy spectrum

In the tight-binding approximation, the electron Hamiltonian in graphene reads

$$H = \sum_{\mathbf{n},\mathbf{m}} t_{\mathbf{nm}}\, a^{+}_{\mathbf{n}} a_{\mathbf{m}}, \qquad (1)$$

where vectors $\mathbf{n}$ and $\mathbf{m}$ denote certain positions on the graphene lattice and Fermi-operators $a^{+}_{\mathbf{n}}$ and $a_{\mathbf{m}}$ create and annihilate electrons at the corresponding places. For the sake of simplicity, we omitted the spin variables in (1). Hopping amplitude $t_{\mathbf{nm}}$ is the matrix element of the operator of kinetic energy. We will consider only two nonzero matrix elements $t \equiv t_{\mathbf{n}\,\mathbf{n}+\rho_{AB}}$ and $t' \equiv t_{\mathbf{n}\,\mathbf{n}+\rho_{AA}} = t_{\mathbf{n}\,\mathbf{n}+\rho_{BB}}$ which describe the nearest and next-to-nearest neighbor hoppings, respectively. Since the graphene's hexagonal lattice can be described in terms of two triangular sublattices A and B, the parameter t is evidently connected with intersublattice hopping and t' with intrasublattice hopping (see Fig. 1).

At low energy, we consider states in the vicinity of the Dirac $\mathbf{K}$ point, $\mathbf{K} = \frac{2\pi}{\sqrt{3}a_{CC}}\left(\frac{2}{3}, 0\right)$, where $a_{CC} = 1.42$ Å is the distance between nearest carbon atoms of the different sublattices. The constant $-3t'$ is omitted, because it can absorbed in chemical potential. Then we retain leading in momentum terms and readily obtain the following effective low energy Hamiltonian defined on two-component spinors whose upper and down components are connected with states on the A and B sublattices, respectively:

$$\hat{H}_{\mathbf{K}}(\mathbf{k}) = \begin{pmatrix} \dfrac{\hbar^2\mathbf{k}^2}{2m^*} & -\hbar v_F(k_x + ik_y) \\ -\hbar v_F(k_x - ik_y) & \dfrac{\hbar^2\mathbf{k}^2}{2m^*} \end{pmatrix}, \qquad (2)$$

where the effective mass and Fermi velocity are

$$m^* = \frac{2\hbar^2}{9t'a_{CC}^2}, \quad v_F = \frac{3ta_{CC}}{2\hbar}. \qquad (3)$$

The effective Hamiltonian for low energy excitations in the vicinity of the Dirac point $\mathbf{K}' = \frac{2\pi}{\sqrt{3}a_{CC}}\left(-\frac{2}{3}, 0\right)$ is obtained from (2) through the replacement $k_x \to -k_x$. One can easily find the spectrum of the Hamiltonian (2)

$$E = \frac{\hbar^2\mathbf{k}^2}{2m^*} \pm \hbar v_F |\mathbf{k}|. \qquad (4)$$

If $t' = 0$ (only the nearest neighbor hopping is retained), then the Hamiltonian (2) together with $H_{\mathbf{K}'}(\mathbf{k})$ is the conventional Dirac Hamiltonian, which is now widely used for the description of electronic properties of graphene. This Hamiltonian has the electron-hole symmetry. Its spectrum is given by the second term on the right-hand side of Eq. (4) and presents the two Dirac cones (near points $\mathbf{K}$ and $\mathbf{K}'$) of positive and negative energies. If, however, $t' \neq 0$, then the electron-hole symmetry is lost and as it is evident from Eq. (4) the spectrum is not symmetric with respect to the change of sign of energy $E \to -E$. Note that in the other limiting case $t = 0$ (only the next-to-nearest neighbor hopping is retained), the Hamiltonian (2) describes conventional nonrelativistic quasiparticles whose spectrum is given by the first term on the right-hand side of Eq. (4). Of course, these limiting cases are quite useful because they help to check calculations performed in the general case.

The Hamiltonian for electron states in a magnetic field in the vicinity of the $\mathbf{K}$ point follows from (2) by using the minimal coupling with electromagnetic field

$$\hat{H}_{\mathbf{K}} = \begin{pmatrix} \dfrac{1}{2m^*}(\hat{\pi}_x^2 + \hat{\pi}_y^2) & -v_F(\hat{\pi}_x + i\hat{\pi}_y) \\ -v_F(\hat{\pi}_x - i\hat{\pi}_y) & \dfrac{1}{2m^*}(\hat{\pi}_x^2 + \hat{\pi}_y^2) \end{pmatrix}, \qquad (5)$$

where $\hat{\boldsymbol{\pi}} = -i\hbar\nabla - ie\mathbf{A}/c$ (obviously, the Hamiltonian for the states in the vicinity of the $\mathbf{K}'$ point is obtained through the replacement $\hat{\pi}_x \to -\hat{\pi}_x$).

It is straightforward to find the spectrum of graphene with t and t' hoppings in a constant magnetic field perpendicular to the graphene plane. The spectrum was first obtained in [7,12] and consists of two non-symmetric branches (see Fig. 2)

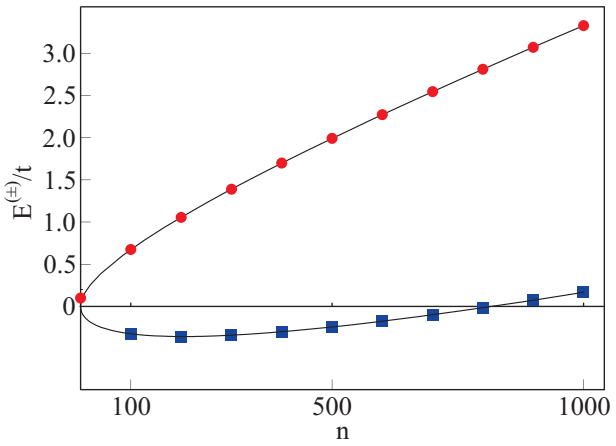

Fig. 2. The spectrum of graphene in units of t, with $t'/t = 0.7$, in magnetic field such that $\frac{1}{t}\sqrt{2v_F^2 \frac{eB\hbar}{c}} = 0.05$, and n is the Landau level index. The dots and squares correspond to the positive $E^{(+)}$ and negative $E^{(-)}$ branches of the spectrum (the square at $n = 0$ is absent according to Eq. (7)).

$$E_n^{(\nu)} = n\hbar\omega_B + \nu\sqrt{\left(\frac{\hbar\omega_B}{2}\right)^2 + 2n\hbar v_F^2 \frac{eB}{c}}, \qquad (6)$$

where $\omega_B = eB/m^* c$ is the standard cyclotron frequency, index ν denotes the upper $\nu = +$ and lower $\nu = -$ branches, $n \geq 1$ is the Landau level index, and we ignore the simple Zeeman linear contribution to energy due to spin. For the lowest Landau level $n = 0$, the energy

$$E_0 = \frac{\hbar\omega_B}{2} \qquad (7)$$

does not depend on t and equals the conventional lowest Landau level energy in the nonrelativistic case.

Note that the lower branch $E_n^{(-)}$ of the spectrum (6) unlike the case of the Dirac spectrum is not monotonic. Let us assume for simplicity that n is continuous. Then, as follows from Eq. (6), for $t' < t'_{\max} = tl_B/\sqrt{27}a_{CC}$ ($l_B = \sqrt{\hbar c/eB}$ is the magnetic length), that is true for graphene in realistic magnetic fields, the energy $E_n^{(-)}$ decreases for small values of n, attains a minimum at

$$E_{\min} = -\frac{m^* v_F^2}{2} - \frac{\hbar^2\omega_B^2}{8m^* v_F^2}, \qquad (8)$$

(since n is discrete, the true minimum of the spectrum (6), in general, is higher than (8)), and then increases for larger values of n (see Fig. 2). At low energies, we stay close to the Dirac points that implies that $|\mathbf{k}|a_{CC} << 1$. This means that we should consider small values of n such that only the decreasing part of the lower branch of the spectrum contributes.

The eigenfunctions of higher Landau levels $n \geq 1$ of the spectrum (6) are given by the following equation below (we use the Landau gauge $\mathbf{A} = (0, xB)$ for the vector potential of the external magnetic field and, as was mentioned above, suppress the spin index):

$$\chi_n^{(\nu)}(x,y) = \frac{\exp(ik_y y)}{\sqrt{2\pi[1+(X_n^{(\nu)})^2]}}\begin{pmatrix}\phi_n(x)\\ -i\phi_{n-1}(x)X_n^{(\nu)}\end{pmatrix}, \qquad (9)$$

where

$$\phi_n(x) = \frac{1}{\sqrt{2^n n! l_B\sqrt{\pi}}}\exp\left[-\frac{1}{2}\left(\frac{x + l_B^2 k_y}{l_B}\right)^2\right] \times$$
$$\times H_n\left(\frac{x + l_B^2 k_y}{l_B}\right), \qquad (10)$$

$H_n(x)$ are Hermite polynomials, and

$$X_n^{(\nu)} = -\frac{v_F\sqrt{2n\hbar\frac{eB}{c}}}{\frac{\hbar\omega_B}{2} + \nu\sqrt{\left(\frac{\hbar\omega_B}{2}\right)^2 + 2n\hbar v_F^2\frac{eB}{c}}}. \qquad (11)$$

Eigenfunctions in the vicinity of the **K'** point have the same factor before the spinor, $i\phi_{n-1}(x)X_n^{(\nu)}$ as the upper component of the spinor, and $\phi_n(x)$ as the lower one.

The eigenfunctions for the lowest Landau level (7) are given by (we assume that $\mathrm{sign}(eB) > 0$ and again, like in the expression (9), suppress the spin variables)

$$\chi_0(x,y) = \frac{\exp(ik_y y)}{\sqrt{2\pi}}\begin{pmatrix}\phi_0(x)\\ 0\end{pmatrix}. \qquad (12)$$

The spectrum (6) has an unusual dependence on the Landau index n and magnetic field B because the energy levels $E_n^{(\nu)}$ cannot be represented as $E_n^{(\nu)} = f_\nu(B(n+\gamma))$, where $f_\nu(x)$ are arbitrary functions and γ is a constant. In Sec. 3, we will see that this leads to the dependence of the frequency of oscillations B_F on the magnetic field B. As well known, B_F does not depend on B in the nonrelativistic and relativistic cases, where the energy spectra have the canonical form $E_n = \hbar\omega_B(n+1/2)$ and $E_n^{(\nu)} = \nu\sqrt{2n\hbar v_F^2 eB/c}$ with $n = 0, 1, 2, .,$ respectively.

What is the reason for this unusual property of spectrum (6), (7)? In order to get an answer to this question, let us first recall why the nonrelativistic and relativistic spectra depend on B only through the combination $B(n+\gamma)$. The nonrelativistic Hamiltonian contains the operator $\hat{\pi}^2$, where $\hat{\pi} = -i\hbar\nabla - ie\mathbf{A}/c$. Its eigenvalue is equal to $2\hbar eB(n+1/2)/c$. The Dirac Hamiltonian contains the operator $\hat{\pi}\gamma$, where γ are the Dirac matrices. At the same time, one can equivalently determine its eigenvalues from $-(\hat{\pi}\gamma)^2 = \hat{\pi}^2 + i\hbar eB\gamma^1\gamma^2/c$. Since $(i\gamma^1\gamma^2)^2 = 1$, the eigenvalues of $i\gamma^1\gamma^2$ are ± 1. Consequent-

ly, eigenvalues of $-(\hat{\pi}\gamma)^2$ are $2\hbar eB(n+1/2)/c \pm \hbar eB/c$. Therefore, the lowest Landau level has zero energy in the relativistic case and higher Landau levels are apparently twice degenerate in view of the twice degenerate spinor part contribution $\pm \hbar eB/c$. Thus, the energy spectrum in the relativistic case like in the nonrelativistic one depends on magnetic field only through the combination $B(n+\gamma)$.

In our case, for electron states of the Hamiltonian (5), the action of the operators $\hat{\pi}_x \pm i\hat{\pi}_y$ and $\hat{\pi}_x^2 + \hat{\pi}_y^2$ on functions $\phi_n e^{ik_y y}$ contains both square root and linear terms in B

$$(\hat{\pi}_x + i\hat{\pi}_y)\phi_n e^{ik_y y} = i\sqrt{\frac{2\hbar|eB|(n+1)}{c}}\,\phi_{n+1} e^{ik_y y},$$

$$(\hat{\pi}_x - i\hat{\pi}_y)\phi_n e^{ik_y y} = -i\sqrt{\frac{2\hbar|eB|n}{c}}\,\phi_{n-1} e^{ik_y y},$$

$$(\hat{\pi}_x^2 + \hat{\pi}_y^2)\phi_n e^{ik_y y} = \frac{\hbar|eB|}{c}(2n+1)\phi_n e^{ik_y y}$$

and, consequently, eigenvalues $E_n^{(\nu)}$ of the Hamiltonian (5) cannot be represented as $f(B(n+\gamma))$.

Finally, we would like to mention that, strictly speaking, the relativistic Hamiltonian for the electron in addition to the Dirac terms contains also an anomalous magnetic moment term $e^2\mu_B/(8\pi^2\hbar c)F_{\mu\nu}\gamma^\mu\gamma^\nu$ (see, e.g., [13]), where μ_B is the Bohr magneton. According to [14], in such a case, the energy spectrum

$$E_n = \left[c^2 p_z^2 + \left(\sigma\frac{e^2\mu_B B}{8\pi^2 c} + \sqrt{(m^* c^2)^2 + \frac{2\hbar eBn}{c}}\right)^2\right]^{1/2},$$

where $\sigma = \pm$ is the electron spin, also does not have the conventional form $f(B(n+\gamma))$ like the energy spectrum (6).

Qualitatively, the most important feature of the spectrum (6), (7) is that it interpolates between the relativistic and nonrelativistic spectra. Indeed, for $\omega_B \to 0$, the spectrum Eqs. (6), (7) reduces to a relativistic spectrum and, for $\omega_B \to \infty$, it tends to a nonrelativistic one. Thus, the next-to-nearest neighbor hopping changes the low energy spectrum of quasiparticles in a system with honeycomb lattice, although, quantitavely this change in real graphene is quite small due to the inequality $t'/t << 1$. Note that the degeneracy of the states of the spectrum (6), (7) coincides with the degeneracy of states of the purely relativistic spectrum. Consequently, the next-to-nearest neighbor hopping in graphene does not change the Berry phase which is connected with the degeneracy of spectrum [15] and equals π. (For $t = 0$, the degeneracy of spectrum is the same as in the nonrelativistic problem and the Berry phase in such a case equals zero.) Therefore, the QHE quantization in odd integers still applies to the case under consideration.

3. The density of states

In the absence of scattering from impurities the quasiparticle DOS can be written as the sum of δ-functions of Landau level energies:

$$D(E) = \frac{2eB}{\pi\hbar c}\left[\delta(E-E_0) + \sum_{n=1,\,\nu=\pm}^{\infty}\delta\,(E-E_n^{(\nu)})\right], \quad (13)$$

or, equivalently,

$$D(E) = \frac{2eB}{\pi\hbar c}\frac{d}{dE}\left[\theta(E-E_0) + \sum_{n=1,\,\nu=\pm}^{\infty}\theta\,(E-E_n^{(\nu)})\right]. \quad (14)$$

Note that $2eB/\pi\hbar c$ is the density of the Landau levels which includes their fourfold valley and spin degeneracy (recall that we suppressed the spin variables contribution to energy which can be easily restored).

Using the Poisson formula

$$\sum_{n=1}^{\infty} f(n) = -\frac{1}{2}f(0) + \int_0^{\infty} f(x)dx + 2\sum_{k=1}^{\infty}\int_0^{\infty} f(x)\cos(2\pi kx)dx, \quad (15)$$

we find

$$\sum_{n=1}^{\infty}\theta(E-E_n^{(+)}) = -\frac{1}{2}\theta(E-E_0) + \theta(E-E_0)\left[x_1 + \sum_{k=1}^{\infty}\frac{1}{\pi k}\sin(2\pi kx_1)\right], \quad (16)$$

for the $\nu = +$ branch of the spectrum and

$$\sum_{n=1}^{\infty}\theta(E-E_n^{(-)}) = -\frac{1}{2}\theta(E+E_0) + \theta(E-E_{\min})\left[x_2 + \sum_{k=1}^{\infty}\frac{1}{\pi k}\sin(2\pi kx_2)\right] + [\theta(E+E_0) - \theta(E-E_{\min})]\left[x_1 + \sum_{k=1}^{\infty}\frac{1}{\pi k}\sin(2\pi kx_1)\right], \quad (17)$$

for the $\nu = -$ branch of the spectrum, where

$$x_j(E) = \frac{v_F^2\hbar eB}{c(\hbar\omega_B)^2} + \frac{E}{\hbar\omega_B} + \frac{(-1)^j}{(\hbar\omega_B)^2}\sqrt{(v_F^2\hbar\frac{eB}{c})^2 + 2\hbar\omega_B v_F^2\frac{\hbar eB}{c}E + \frac{(\hbar\omega_B)^4}{4}}, \quad (18)$$

$$j = 1, 2.$$

It is easy to check that $x_j(E)$ correspond to two inverse functions $n_j(E)$ which can be found from Eq. (6). The presence of two functions $x_j(E)$ is due to the fact that for $E > E_{\min}$ (where $E_{\min}$ is defined in Eq. (8)), a given energy corresponds to two points in the spectrum (see Fig. 2). The function $x_1(E)$ denotes intersection of the line of constant energy with the $\nu = +$ branch of the spectrum or with the decreasing part of the $\nu = -$ branch. The function $x_2(E)$ corresponds to intersection with the increasing part of the $\nu = -$ branch. Therefore, the sum over the $\nu = +$ branch of spectrum given by Eq. (16) contains only $x_1(E)$ unlike Eq. (17) for the $\nu = -$ branch of the spectrum which, for $E_{\min} \le E \le -E_0$, contains terms with both $x_1(E)$ and $x_2(E)$. For $E > -E_0$, the line of constant energy intersects only the increasing part of the $\nu = -$ branch, therefore, only the term with $x_2(E)$ in (17) contributes in this case.

Combining Eqs. (14), (16) and (17) we obtain the exact DOS for the spectrum (6), (7)

$$D(E) = \frac{2eB}{\pi\hbar c}\frac{d}{dE}\left\{\frac{1}{2}\theta(E-E_0) - \frac{1}{2}\theta(E+E_0) + \right.$$
$$+ \theta(E-E_{\min})\left[x_2 + \sum_{k=1}^{\infty}\frac{1}{\pi k}\sin(2\pi k x_2)\right] + [\theta(E+E_0) +$$
$$\left. + \theta(E-E_0) - \theta(E-E_{\min})]\left[x_1 + \sum_{k=1}^{\infty}\frac{1}{\pi k}\sin(2\pi k x_1)\right]\right\}. \quad (19)$$

According to the discussion in Sec. 2, since x is continuous, $E_{\min}$, in general, is not equal to the lowest energy level of the spectrum (6), (7), where n is discrete. The expression in the curly brackets in (19) is nonzero for $E > E_{\min}$. Therefore, it is not immediately clear that the DOS given by Eq. (19) is zero for energies between $E_{\min}$ and the true lowest level of the spectrum (6),(7). To prove this, it is useful to recall [19] that the first Bernoulli polynomial in the interval $0 < x < 1$ can be expressed as follows:

$$B_1(x) = x - \frac{1}{2} = -\sum_{k=1}^{\infty}\frac{1}{\pi k}\sin(2\pi k x). \quad (20)$$

For x beyond the interval $[0, 1]$, in order to find the sum over $\sin(2\pi k x)$ functions, one can use the first Bernoulli polynomial periodically continued beyond the interval $x \in [0, 1]$ which depends on the fractional part of its argument, i.e. $B_1(x - [x])$. Here, $[x]$ is the largest integer satisfying $[x] \le x$. Thus, we obtain

$$\sum_{k=1}^{\infty}\frac{1}{\pi k}\sin(2\pi k x) = -B_1(x-[x]) = \frac{1}{2} - x + [x].$$

As result, the function

$$x + \sum_{k=1}^{\infty}\frac{1}{\pi k}\sin(2\pi k x) = \frac{1}{2} + [x]$$

has a staircase-like behavior (see Fig. 3).

It is not surprising at all that we obtained this result. Our DOS (19) is given as a full derivative with respect to E. Integrating it over E, one finds the number of states. Consequently, the quantity in the curly brackets in Eq. (19) up to a factor coincides with the number of states. Since the spectrum in a magnetic field is discrete, this quantity should have a staircase-like behavior. Therefore, the DOS is not equal zero only when E crosses some energy level of the system. When this happens, the expression in the curly brackets in Eq. (19) experiences a jump between different plateaus.

As it was mentioned at the end of Sec. 2, we should consider only rather small values of n. This implies that only terms with x_1 should be retained in Eq. (19) and all terms with x_2 can be omitted because they correspond to states with very large n. Thus, we arrive at the following final expression for the physically relevant DOS in graphene:

$$D(E) = \frac{2eB}{\pi\hbar c}\frac{d}{dE}\left\{\frac{1}{2}\theta(E-E_0) - \frac{1}{2}\theta(E+E_0) + [\theta(E+E_0) + \right.$$
$$\left. + \theta(E-E_0) - \theta(E-E_{\min})]\left([x_1] + \frac{1}{2}\right)\right\}. \quad (21)$$

The customary form (see, e.g., [16]) of x_1 is $x_1 = \hbar c S(E)/(2\pi eB) - \gamma$, where $S(E)$ is the semiclassical electron orbit area in the space of wave vector k, and $\gamma = 1/2 - \phi_B/2\pi$ with ϕ_B being the Berry phase. According to the results of the previous section, the Berry phase for the system under consideration equals π and, consequently, $\gamma = 0$. Therefore, using (18), one finds that the analog of the semiclassical electron orbit in our case is

$$\frac{\hbar^2}{2\pi}S(E) = v_F^2(m^*)^2 + Em^* -$$
$$- v_F^2(m^*)^2\sqrt{1 + \frac{2E}{m^* v_F^2} + \frac{\hbar^2 e^2 B^2}{4(m^*)4v_F^4 c^2}}. \quad (22)$$

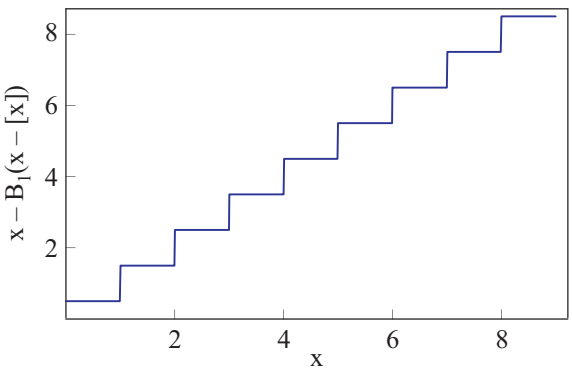

Fig. 3. The function $x - B_1(x - [x])$.

The fact that Eq. (22) depends on magnetic field B means that $S(E)$ cannot be interpreted as a semiclassical electron orbit. This unusual form of $S(E)$ is connected with the unconventional dependence of the energy levels (6) on the Landau level index and magnetic field discussed in the previous section. Moreover, we will see in the next section, where we plot the fan diagram, that the unusual character of the dependency of x_1 on B is responsible for the unconventional form of the fan diagram for our system which is not a straight line unlike the well known cases of nonrelativistic and relativistic systems.

Finally, we would like to note that $S(E)$, given by Eq. (22), tends to the correct value of semiclassical electron orbit area $\pi E^2/(\hbar^2 v_F^2)$ [16] in the relativistic limit $t' \to 0$. In the nonrelativistic limit $t \to 0$, the function $S(E)$, given by Eq. (22), tends to $2\pi E m^*/\hbar^2 - \pi eB/(\hbar c)$, where $2\pi E m^*/\hbar^2$ is the correct nonrelativistic semiclassical electron orbit area and, obviously, the second term $-\pi eB/(\hbar c)$ multiplied by $\hbar c/(2\pi eB)$ gives the standard nonrelativistic value $\gamma = 1/2$ [16]. Note that, although Eq. (22) tends smoothly to the relativistic and nonrelativistic expressions in the corresponding limits, the Berry phase does not have such a smooth behavior. It equals π for any nonzero t and abruptly jumps to zero when t exactly equals zero. This behavior of the Berry phase is connected with its topological character [10].

4. Fan diagrams

Fan diagrams are a standard [2,17] and convenient way to display graphically information about the spectrum of the system. They express the inverse magnetic field B^{-1} as function of the Landau level index n at some fixed chemical potential μ.

For the $\nu = +$ branch of the spectrum (6), we find

$$\frac{1}{B} = \left(\frac{\hbar e}{m^*\mu c} + \frac{v_F^2 \hbar e}{\mu^2 c}\right) n + \frac{v_F^2 \hbar e}{\mu^2 c}\sqrt{\left(\frac{2\mu}{m^* v_F^2} + 1\right) n^2 + \frac{\mu^2}{4(m^*)^2 v_F^4}}\,. \qquad (23)$$

For $t = 0$, Eq. (23) reduces to

$$\frac{1}{B} = \frac{\hbar e}{cm^*\mu}\left(n + \frac{1}{2}\right) = \frac{4}{\phi_0 \rho_{nr}}\left(n + \frac{1}{2}\right), \qquad (24)$$

where in the last equality we used the relation $\rho_{nr} = 2\mu m^*/(\pi\hbar^2)$ between carrier density ρ_{nr} and chemical potential μ in the nonrelativistic case ($\phi_0 = hc/e$ is the flux quantum). For $t' = 0$, Eq. (23) gives

$$\frac{1}{B} = \frac{2e\hbar v_F^2}{c\mu^2} n = \frac{4}{\phi_0 \rho_{\rm rel}} n\,, \qquad (25)$$

where in the last equality we expressed μ via the relativistic carrier density $\rho_{\rm rel} = \mu^2/(\pi\hbar^2 v_F^2)$. Equations (24) and (25) illustrate the well-known fact that the fundamental frequency $B_F = \phi_0 S(E)/(4\pi^2)$ of quantum magnetic oscillations for any 2D system is defined by its degeneracy f and the concentration of electrons or holes ρ; so that $B_F = \phi_0 \rho / f$. For graphene $f = 4$ because of double-spin and double-valley degeneracy.

For $n >> 1$, Eq. (23) implies that

$$\frac{1}{B} = \left[\frac{\hbar e}{m^*\mu c} + \frac{v_F^2 \hbar e}{\mu^2 c}\left(\sqrt{1 + \frac{2\mu}{m^* v_F^2}} + 1\right)\right] n + O\left(\frac{1}{n}\right). \qquad (26)$$

Since a constant term (the term which does not depend on n) is absent in (26), the dependence of B^{-1} on n is the same as in Eq. (25) for the relativistic case with $t' = 0$. Matching slopes of the dependencies $B^{-1}(n)$ in Eqs. (24), (25), and (26) gives

$$\rho_{\rm rel} = \rho_{\rm nr} = \frac{4}{\phi_0\left[\frac{\hbar e}{m^*\mu c} + \frac{v_F^2 \hbar e}{\mu^2 c}\left(\sqrt{1 + \frac{2\mu}{m^* v_F^2}} + 1\right)\right]}\,. \qquad (27)$$

Using Eq. (27), we plot in Fig. 4 the fan diagrams for the system under consideration (23) and the nonrelativistic and relativistic systems given by Eqs. (24) and (25), respectively. The most important property of the fan diagram for the system under consideration is that it is not a straight line unlike the fan diagrams for the nonrelati-

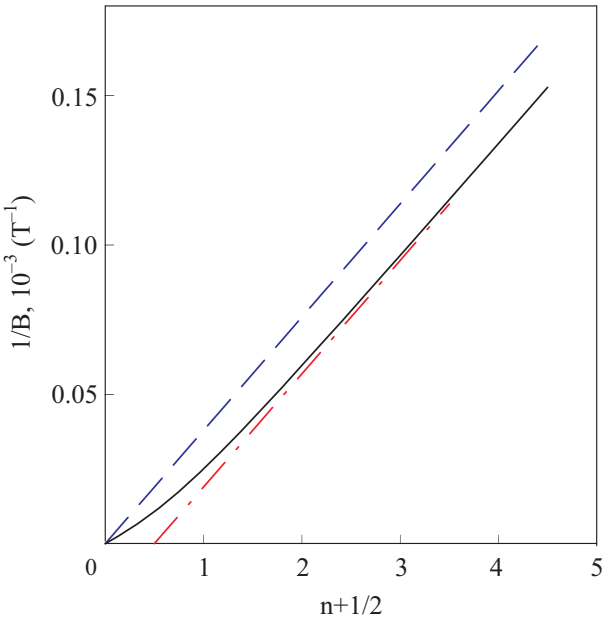

Fig. 4. Fan diagrams for the $\nu = +$ branch of the spectrum (solid line) with parameters $t' = 1.89$ eV, $t = 2.7$ eV, $\mu = 11.5$ eV , the relativistic system $t' = 0$, $t = 2.7$ eV, $\mu_r = 5$ eV (dash-dotted line), and the nonrelativistic system $t = 0$, $t' = 1.89$ eV, $\mu_{nr} = 6.5$ eV (dashed line). Integer values of n denoted by dots correspond to the Landau level index in the spectrum.

vistic and relativistic systems separately. As we have already mentioned in the previous section, this fact is due to the unconventional dependency of x_1 on B which in its turn is connected with the unusual dependency of the spectrum (6) on B. According to Fig. 4, the fan diagram for our system (solid line) interpolates between the fan diagrams for the nonrelativistic and relativistic systems. Namely, it intersects the nonrelativistic fan diagram (dashed line) at the origin and tends to the relativistic fan diagram (dash-dotted line) for large n.

5. Discussion and conclusion

In the present work we have taken into account the next-to-nearest neighbor hopping in graphene in the tight-binding approximation. For the states in the vicinity of the Dirac points, we have considered the off-diagonal sublattice terms of the Hamiltonian up to the first order in momentum and the diagonal sublattice terms up to the second order. The advantage of the effective Hamiltonian (2) is that it leads to the model exactly solvable in an external magnetic field whose Hamiltonian is given by Eq. (5) and the energy spectrum by Eqs. (6), (7). For this model, we have calculated the DOS (19) and ploted the fan diagram (Fig. 4), which interpolates between the fan diagrams for the relativistic and nonrelativistic systems. We have shown that the Berry phase for the model under consideration equals π, i.e. coincides exactly with the Berry phase for the relativistic system.

In a recent paper [21] a related problem was studied. There both the off-diagonal and diagonal terms of the Hamiltonian were considered up to the third order in momentum. The corresponding energy dispersion includes not only the contribution due to the next-to-nearest neighbor hopping (see Eq. (4)), but also high-order band corrections such as trigonal warping terms. It turns out, however, that in an external magnetic field the warping terms do not contribute to the spectrum. Accordingly, the spectrum (6) agrees with the spectrum derived in Ref. 21 in the large-n limit up to the terms $\sim n^{3/2}$. The only essential difference is that the large-n limit misses the n-independent term under the square root in Eq. (6) which is responsible for the recovery of the zero Berry phase in the nonrelativistic, $t = 0$, limit.

The experimental results reported in Ref. 21 indicate that at energies above 500 meV a deviation from the ideal behavior of the Dirac quasiparticles is observed. However, the asymmetry between the valence and conduction bands studied here seems to play a minor role as compared to the trigonal warping of the Fermi surface.

Acknowledgements

The authors are grateful to V.P. Gusynin for stimulating discussions. The work of E.V.G. was supported by the SCOPES project IB 7320-110848 of the Swiss NSF, the grant 10/07-N «Nanostructure systems, nanomaterials, nanotechnologies», the Program of Fundamental Research of the Physics and Astronomy Division of the National Academy of Sciences of Ukraine, and by the State Foundation for Fundamental Research of Ukraine (grant F16-457-2007).

1. K.S. Novoselov, A.K. Geim, S.V. Morozov, D. Jiang, Y. Zhang, S.V. Dubonos, I.V. Grigorieva, and A.A. Firsov, *Science* **306**, 666 (2004).
2. K.S. Novoselov, A.K. Geim, S.V. Morozov, D. Jiang, M.I. Katsnelson, I.V. Grigorieva, S.V. Dubonos, and A.A. Firsov, *Nature* **438**, 197 (2005).
3. Y. Zhang, Y.-W. Tan, H.L. Störmer, and P. Kim, *Nature* **438**, 201 (2005).
4. Y. Zheng and T. Ando, *Phys. Rev.* **B65**, 245420 (2002).
5. V.P. Gusynin and S.G. Sharapov, *Phys. Rev. Lett.* **95**, 146801 (2005).
6. V.P. Gusynin and S.G. Sharapov, *Phys. Rev.* **B73**, 245411 (2006).
7. N.M.R. Peres, F. Guinea, and A.H. Castro Neto, *Phys. Rev.* **B73**, 125411 (2006).
8. P.R.Wallace, *Phys. Rev.* **71**, 622 (1947).
9. G. Semenoff, *Phys. Rev. Lett*. **53**, 2449 (1984).
10. M.V. Berry, *Proc. R. Soc. London* **A392**, 45 (1984).
11. P. Carmier and U. Denis, *arXiv:0801.4727 [cond-mat. meshall]*.
12. Yu.B. Gaididei and V.M. Loktev, *Fiz. Nizk. Temp.* **32**, 923 (2006) [*Low Temp. Phys.* **32**, 703 (2006)].
13. C. Itzykson and J.-B. Zuber, *Quantum Field Theory*, McGraw-Hill, New York (1980).
14. I.M. Ternov, V.G. Bagrov, and V.Ch. Zhukovsky, *Vestn. Mosk. Univ*., *Ser. 3: Fiz., Astron.* **1**, 30 (1966).
15. D.N. Sheng, L. Sheng, and Z.Y. Weng, *Phys. Rev.* **B73**, 233406 (2006).
16. I.A. Luk`yanchuk and Ya. Kopelevich, *Phys. Rev. Lett.* **93**, 166402 (2004).
17. Y. Zhang, J.P. Small, M.E.S. Amori, and P. Kim, *Phys. Rev. Lett.* **94**, 176803 (2005).
18. S.G. Sharapov and V.P. Gusynin, H. Beck, *Phys. Rev.* **B69**, 075104 (2004).
19. I.S. Gradshtein and I.M. Ryzhik, *Table of Integrals, Series and Products*, Academic Press, (2000).
20. H.K. Nguyen and S. Chakravarty, *Phys. Rev.* **B65**, 180519 (2002).
21. P. Plochocka, C. Faugeras, M. Orlita, M.L. Sadowski, G. Martinez, M. Potemski, M.O. Goerbig, J.-N. Fuchs, C. Berger, and W.A. de Heer, *Phys. Rev. Lett.* **100**, 087401 (2008).